Original Article

Comparison between diaphragmatic-navigated and self-navigated coronary magnetic resonance angiography at 3T in pediatric patients with congenital coronary artery anomalies

Shiganmo Azhe[1,2#], Xuesheng Li[1#], Zhongqin Zhou[1,2], Chuan Fu[1], Yun Wang[1], Xiaoyue Zhou[3], Jing An[4], Davide Piccini[5,6], Jessica Bastiaansen[7,8], Yingkun Guo[1,2], Lingyi Wen[1,2]

[1]Department of Radiology, West China Second University Hospital, Sichuan University, Chengdu, China; [2]Key Laboratory of Birth Defects and Related Diseases of Women and Children (Sichuan University), Ministry of Education, West China Second University Hospital, Sichuan University, Chengdu, China; [3]MR Collaboration, Siemens Healthineers Ltd., Shanghai, China; [4]Siemens Shenzhen Magnetic Resonance Ltd., Shenzhen, China; [5]Department of Diagnostic and Interventional Radiology, Lausanne University Hospital and University of Lausanne, Lausanne, Switzerland; [6]Advanced Clinical Imaging Technology, Siemens Healthcare AG, Lausanne, Switzerland; [7]Department of Diagnostic, Interventional and Paediatric Radiology, Inselspital, University Hospital Bern, University of Bern, Bern, Switzerland; [8]Translation Imaging Center (TIC), Swiss Institute for Translational and Entrepreneurial Medicine, Bern, Switzerland

Contributions: (I) Conception and design: S Azhe, X Li, L Wen, Z Zhou; (II) Administrative support: Y Guo, L Wen; (III) Provision of study materials or patients: X Zhou, J An, D Piccini, J Bastiaansen, C Fu, Y Wang; (IV) Collection and assembly of data: S Azhe, X Li; (V) Data analysis and interpretation: S Azhe, L Wen; (VI) Manuscript writing: All authors; (VII) Final approval of manuscript: All authors.

[#]These authors contributed equally to this work as co-first authors.

Correspondence to: Lingyi Wen, MD, PhD. Department of Radiology, West China Second University Hospital, Sichuan University, Chengdu 610041, China; Key Laboratory of Birth Defects and Related Diseases of Women and Children (Sichuan University), Ministry of Education, West China Second University Hospital, Sichuan University, No. 20 South Renmin Road, Chengdu 610041, China. Email: lizzievane@126.com.

Background: Coronary magnetic resonance angiography (CMRA) is being increasingly used in pediatric patients with congenital coronary artery anomalies (CAAs). However, the data on the free-breathing self-navigation technique, which has the potential to simplify the acquisition plan with a high success rate at 3T, remain scarce. This study investigated the clinical application value of self-navigated (sNAV) CMRA at 3T in pediatric patients with suspected CAAs and compared it to conventional diaphragmatic-navigated (dNAV) CMRA.

Methods: From April 2019 to March 2022, we enrolled 65 pediatric patients (38 males and 27 females; mean age 8.5±4.4 years) with suspected CAAs in this prospective study. All patients underwent both dNAV and sNAV sequences in random order with gradient recalled echo (GRE) sequence during free breathing, with 39 (20 males and 19 females; mean age 10.2±3.6 years) of them additionally undergoing coronary computed tomography angiography (CCTA) or invasive coronary angiography (ICA). We measured and compared the success rate, scan time, visual score of the 9 main coronary artery segments, vessel sharpness, and vessel length between the two sequences. The diagnostic accuracy was compared using CCTA or ICA as a reference.

Results: The success rate of sNAV-CMRA (65/65, 100%) was higher than that of dNAV-CMRA (61/65, 93.8%) (P<0.001), and the scan time of sNAV-CMRA (7.3±2.5 min) was significantly shorter than that of dNAV-CMRA (9.1±3.6 min) (P=0.002). The acquisition efficiency of dNAV-CMRA was 40.5%±12.9%, while for sNAV-CMRA, 100% acquisition efficiency was achieved. There was no significant difference in vessel length of any of the coronary arteries, visual score, or vessel sharpness of the left circumflex coronary artery (LCX) between the two sequences (all P values >0.050). The visual score and vessel sharpness of the right coronary artery and left anterior descending coronary artery (LAD) were significantly improved

in dNAV-CMRA compared with sNAV-CMRA (all P values <0.050). The sensitivity, specificity, positive predictive value (PPV), and negative predictive value (NPV) for the detection of CAAs were not significantly different between the two sequences (all P values >0.050).

Conclusions: Our findings demonstrated that both sNAV and dNAV in CMRA provide clinical application value in pediatric patients with CAAs and have similar diagnostic performance. Although the image quality of sNAV-CMRA is slightly inferior compared to that of dNAV-CMRA, sNAV-CMRA allows for a simpler scanning procedure.

Keywords: Self-navigation; diaphragmatic-navigation; coronary magnetic resonance angiography (CMRA); congenital coronary artery anomalies (CAAs)

Submitted Apr 24, 2023. Accepted for publication Oct 07, 2023. Published online Oct 26, 2023.
doi: 10.21037/qims-23-556
View this article at: https://dx.doi.org/10.21037/qims-23-556

Introduction

Coronary artery anomalies (CAAs) encompass several congenital conditions, including the abnormal origin of the main coronary artery and an anomalous course, with prevalence ranging from 0.2% to 5.8% (1). CAAs (2), especially anomalous coronary artery originating from the opposite sinus of Valsalva (ACAOS) with an interarterial course (3), may contribute to myocardial ischemia and sudden cardiac death in young adults and children. The clinical meaning of CAAs varies significantly depending on the artery involved origin and course (1). Thus, the accurate diagnosis of CAAs is essential for risk stratification and selection of the therapeutic approach. Although invasive coronary angiography (ICA) and coronary computed tomography angiography (CCTA) are the reference standards for diagnosing CAAs, their use in children is limited due to invasiveness and exposure to high radiation doses or iodinated contrast agents (4). Echocardiography is commonly used to evaluate CAAs in children but is limited in identifying coronary artery ostia and the surrounding structures (5).

Coronary magnetic resonance angiography (CMRA) is a noninvasive and radiation-free imaging modality that has proven valuable in diagnosing CAAs (6,7). The clinical guidelines recommend that CMRA be applied in pediatric patients with CAAs for diagnosis and preoperative planning (class I, level of evidence B) (8). The most common conventional approach to correcting respiratory motion is a diaphragmatic-navigated (dNAV) CMRA. However, this technique is limited due to its long scan time (9,10), a high risk of failure, and complex scan planning (11). To address these limitations, Piccini *et al.* proposed the 3D radial spiral phyllotaxis sampling scheme self-navigated CMRA (sNAV-CMRA) sequence, which integrates both an intrinsic readout arrangement that minimizes eddy current effects, and designed an overall uniform readout distribution (12). By directly extracting data from the heart to correct motion, sNAV achieves 100% acceptance of the acquired data (13), simplifying the acquisition plan without the need to use a diaphragm navigator, simultaneously improving the scan success rate and reducing the acquisition time. Moreover, lipid-insensitive binomial off-resonant excitation radiofrequency excitation (LIBRE) is pulsed to respiratory sNAV 3D radial whole-heart sequence at 3T, which has been demonstrated to enable robust large volume fat suppression and significantly improve coronary artery image quality (14).

In pediatric patients, the clinical application of CMRA is challenging due to their faster heart rate, smaller vessel size, poor cooperation, and irregular respiration. Increasing the availability of higher field strength, such as in 3T magnetic resonance imaging (MRI), enables submillimetric spatial resolution, higher temporal resolution, and better contrast-to-noise ratio (CNR) (15,16). Recently, 3T scanners have become increasingly used in clinical practice. Several researchers have reported that noncontrast and post-contrast sNAV-CMRA at 1.5T was highly accurate for diagnosing CAAs (17,18). However, data for CMRA at 3T remains scarce, and the clinical application of 3T CMRA remains to be investigated in the clinical context of pediatric patients with suspected CAAs. Thus, this study aimed to determine the clinical application value of 3T sNAV-CMRA in pediatric patients with CAAs and to compare it to that of conventional dNAV-CMRA. The scan time, success rate, and image quality, as well the diagnostic value in detecting

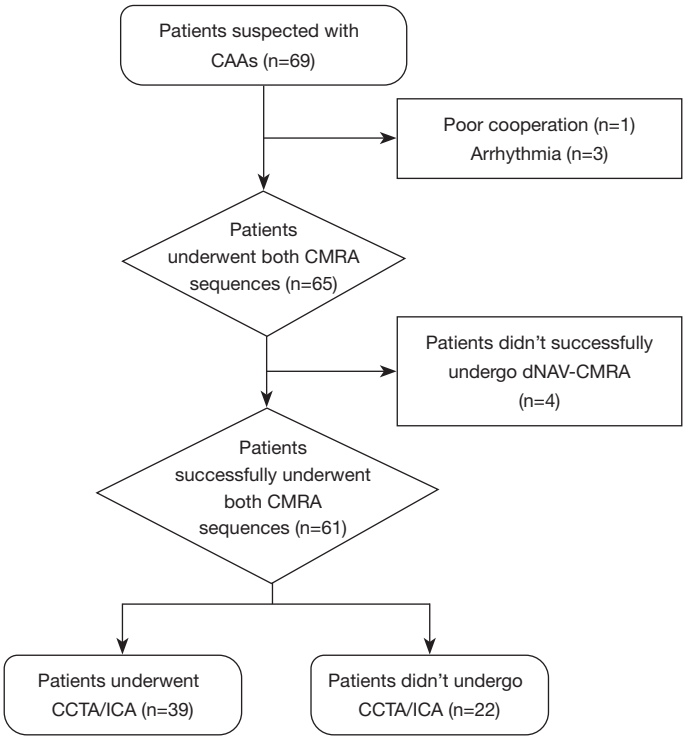

Figure 1 Flowchart of study participant inclusion according to study eligibility criteria. CAA, coronary artery anomaly; CMRA, coronary magnetic resonance angiography; dNAV-CMRA, diaphragmatic-navigated coronary magnetic resonance angiography; CCTA, coronary computed tomography angiography; ICA, invasive coronary angiography.

CAAs using CCTA or ICA as the reference, were compared between dNAV-CMRA and sNAV-CMRA in pediatric patients with suspected CAAs.

Methods

Study population

This prospective study was conducted in accordance with the Declaration of Helsinki (as revised in 2013) and approved by the Ethics Committee of the Sichuan University (No. KL108). Written informed consent was obtained from each patient's legal guardian before enrollment. From April 2019 to March 2022, consecutive pediatric patients suspected to have CAAs according to the European Society of Cardiology's guidelines (1) were enrolled in this study. The exclusion criteria were arrhythmia, metallic implants, and severe claustrophobia. The inclusion flowchart of the study population is shown in *Figure 1*.

CMRA protocol

All examinations were performed with a 3T MRI system (MAGNETOM Skyra; Siemens Healthineers, Erlangen, Germany). Patients younger than 6 years old were examined under sedation according to clinical request. An 18-channel receiver body array coil with a spine array coil was used. Acquisitions were triggered with electrocardiography (ECG). Localization images of the heart were obtained in the three orthogonal directions. Two-dimensional cine in 4-chambers with balanced steady-state free precession (bSSFP) sequence was performed to assess the relatively static period of the right coronary artery (RCA) during the cardiac cycle to determine the trigger delay time and acquisition window. The detailed parameters of the cine sequence were detailed in a previous study (19). We optimized both navigator-gated and respiratory sNAV whole-heart CMRA protocols that balanced the spatial resolution, signal-to-noise ratio (SNR), and scan time in clinical practice (20). We performed a phantom experiment

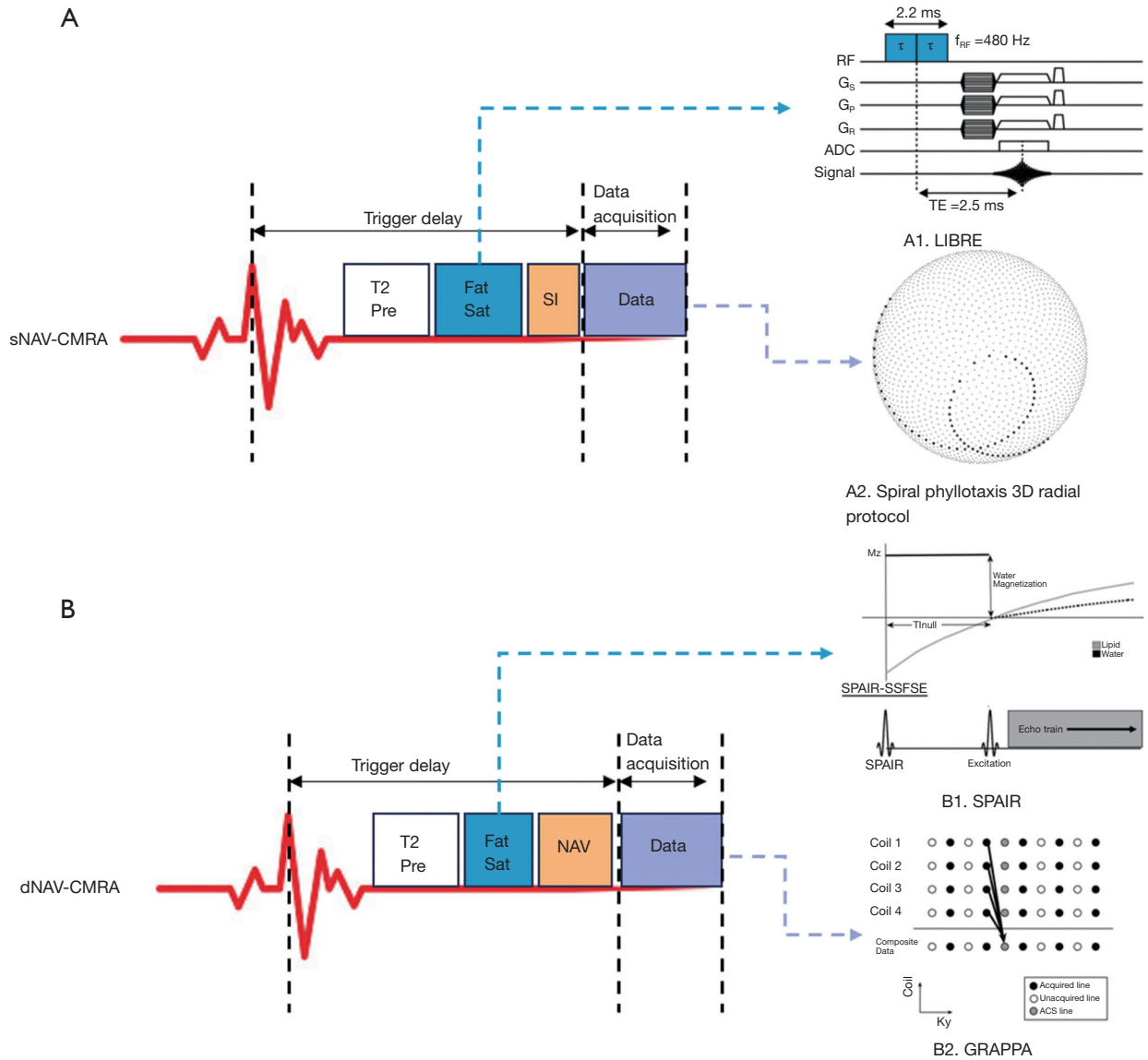

Figure 2 Diagram of the different components of the dNAV and sNAV sequence. (A) In the sNAV-CMRA, the fat-saturation technique LIBRE [A1 reprinted with permission from Bastiaansen *et al.* (14)] and the segmented 3D radial spiral phyllotaxis sampling scheme [A2 reprinted with permission from Piccini *et al.* (21)] were used in sNAV. (B) In the dNAV-CMRA, the fat-saturation technique SPAIR [B1 reprinted with permission from Lauenstein *et al.* (22)] and the traditional GRAPAA technique [B2 reprinted with permission from Griswold *et al.* (23)] were used in dNAV. sNAV-CMRA, self-navigated coronary magnetic resonance angiography; T2 Prep, T2 preparation; Fat Sat, fat-saturation prepulses; SI, superior-inferior; RF, radio frequency; ADC, apparent diffusion coefficient; TE, echo time; LIBRE, lipid-insensitive binomial off-resonant excitation radiofrequency excitation; dNAV-CMRA, diaphragmatic-navigated coronary magnetic resonance angiography; NAV, navigator; SPAIR, spectral-attenuated inversion recovery; ACS, auto-calibration signal; GRAPAA, generalized autocalibrating partially parallel acquisitions.

to investigate the influence of different imaging parameters and strategies of the two sequences on image quality (see Figure S1). The diagram of the two sequences is shown in *Figure 2*. Both the dNAV and sNAV approaches were acquired in randomized order with gradient recalled echo (GRE) sequences during free breathing. Both sequences

Table 1 The parameters of dNAV-CMRA and sNAV-CMRA

Parameter	dNAV-CMRA	sNAV-CMRA
Sampling scheme	3D Cartesian (centric ordering)	3D radial sampling (spiral phyllotaxis)
Acceleration technique	GRAPPA, acceleration factor 2	~20% of radial Nyquist limit acquired, acceleration factor 5
FOV (mm^2)	290×190	220×220
Spatial resolution (mm^3)	1.14×1.14×1.0	1.13×1.13×1.13
TE/TR (ms)	1.74/3.9	2.76/6
Receiver bandwidth (Hz/pixel)	610	606
Accept window (mm)	±2.0	N/A
Image matrix	256×168	192×192
Flip angle (°)	20	20
T2 preparation (ms)	50	40
Slice thickness (mm)	1	1.15
Fat suppression	SPAIR	LIBRE
Radial views	–	11,184
Undersampling rate (%)	–	20
Reconstruction technique	GRAPPA	Nonuniform FFT with zero-filling including uniformly distributed density compensation

dNAV-CMRA, diaphragmatic-navigated coronary magnetic resonance angiography; sNAV-CMRA, self-navigated coronary magnetic resonance angiography; FOV, field of view; TE/TR, time of echo/time of repetition; GRAPPA, generalized autocalibrating partially parallel acquisitions; SPAIR, spectral-attenuated inversion recovery; N/A, not applicable; LIBRE, lipid-insensitive binomial off-resonant excitation; FFT, fast Fourier transform.

were performed 12–15 min post-contrast without additional dedicated contrast agent administration.

For dNAV-CMRA, an ECG-triggered, fat-saturated, segmented, 3D GRE sequence was employed. The 3D k-space data were collected with Cartesian sampling (centric ordering). The parallel imaging technique (GRAPPA) was used with an acceleration factor of 2 to accelerate data acquisition (23). A cross-pair dNAV with an acceptance window of ±2 mm located at the dome of the right hemidiaphragm was used to monitor the movement of the diaphragm, and a tracking factor of 0.6 was used to reduce respiratory artifacts (24). The spectral-attenuated inversion recovery (SPAIR) product fat-saturation technique (25) and T2 preparation pulse were also used for blood-to-myocardium contrast optimization (26). The data were reconstructed with GRAPPA (23). The parameters of the dNAV-CMRA and sNAV-CMRA protocol are shown in *Table 1*.

For sNAV-CMRA, an ECG-triggered, segmented, prototype sNAV, 3D GRE sequence (Siemens Healthineers) was employed (12,20,27). The sequence uses 3D radial sampling with a spiral phyllotaxis pattern, which has proven to be less sensitive to motion compared to the conventional cartesian readout (12). Data corresponding to ~20% of the radial Nyquist limit were acquired (5-fold acceleration) (12). The T2 preparation pulse and the LIBRE fat-suppression technique were used to optimize contrast (14). A saturation slab was accurately placed on the anterior chest wall to suppress the fat signal from the chest (21). The bright signal originating from the blood pool along the superior-inferior direction was acquired at each heartbeat and used for respiratory motion correction. The data were reconstructed with a nonuniform fast Fourier transform (non-uniform FFT) with zero-filling, which included uniformly distributed density compensation (21). Other detailed parameters are shown in *Table 1*.

CCTA protocol

CCTA images were obtained using a CT scanner (GE HealthCare, Chicago, IL, USA) within 2 weeks of CMRA examination. All the patients were examined in the supine

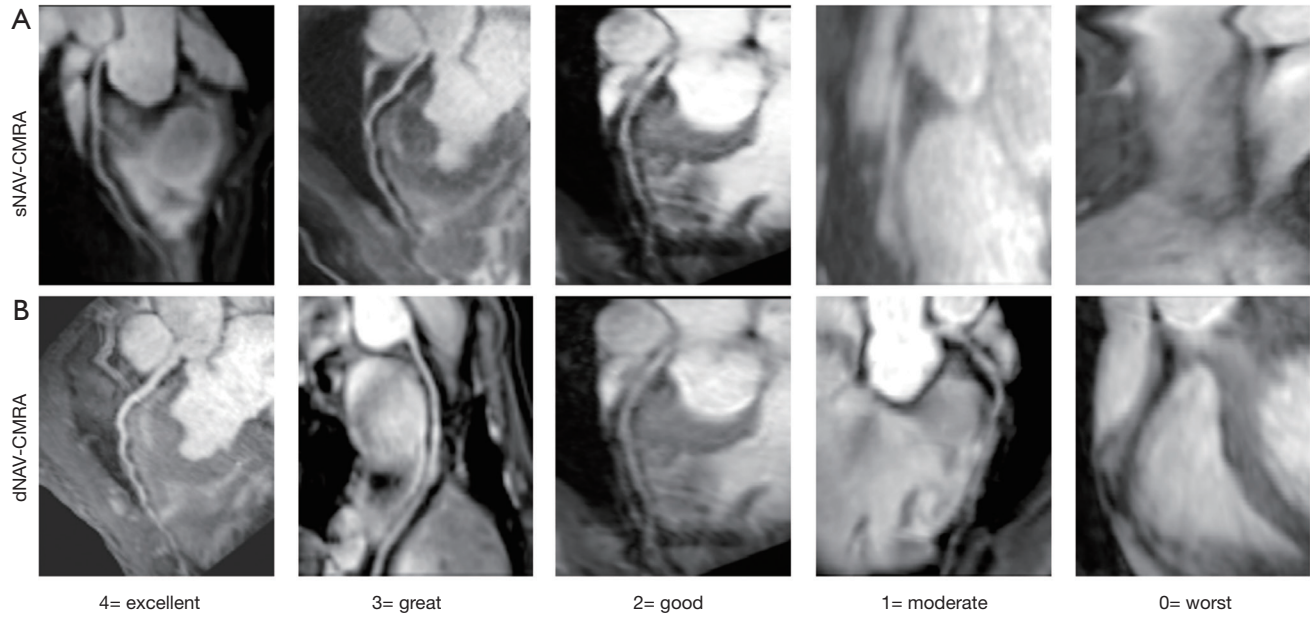

Figure 3 Illustration of visual scoring of the coronary artery of sNAV-CMRA and dNAV-CMRA. (A) Visual score scale of sNAV-CMRA. (B) Visual score scale of dNAV-CMRA. 0= worst, coronary artery poorly visualized; 1= moderate, coronary artery visible but with marked blurring; 2= good, coronary artery visible with moderate blurring; 3= great, coronary artery visible with mild blurring; 4= excellent, coronary artery visible with sharp edges. sNAV-CMRA, self-navigated coronary magnetic resonance angiography; dNAV-CMRA, diaphragmatic-navigated coronary magnetic resonance angiography.

position, and image acquisitions were prospectively ECG-gated. Sedation was used in children who could not cooperate with the examination. The iodinated contrast agent (omnipaque, 1 mL/kg) was intravenously injected. The other parameters were as follows: detector coverage, 100 mm/circle; tube voltage, 80–100 kV; automatic tube current; slice thickness, 0.625 mm; and temporal resolution, 0.28 s. Images were reconstructed in the optimal systolic or diastolic periods after examination with an AW VolumeShare 7 post-processing workstation (GE HealthCare). An experienced radiologist assessed the CAAs.

ICA

A standard invasive coronary angiographic examination was performed on an Allura Xper FD20 catheterization system (Philips, Amsterdam, The Netherlands) within 2 weeks of the CMRA examination. An experienced cardiologist evaluated the presence of CCAs.

CMRA image quality analysis

CMRA image interpretations were performed on an offline workstation (cvi42; Circle Cardiovascular Imaging, Inc., Calgary, AB, Canada). The dNAV-CMRA and sNAV-CMRA datasets were assessed by two experienced (Azhe S and Zhou Z) cardiovascular radiologists using transverse and curved planar reconstruction (CPR). In addition, the radiologists were blinded to the clinical information and the results of CCTA and ICA. Indeterminate CMRA tests were considered to be diagnostic errors.

A model of 18 coronary artery segments from the guidelines of the Society of Cardiovascular Computed Tomography (28) was used in our study. The visualization of the coronary artery segment was assessed on a 5-point scale according to the following scheme: 0= worst (artery not visible); 1= moderate (coronary artery visible, with markedly blurred borders or edges); 2= good (coronary artery visible, with moderately blurred boundaries or edges); 3= great (coronary artery visible, with mildly blurred borders or edges); and 4= excellent (coronary artery visible, with sharply defined borders or edges) (17). The score scale in our study is shown in *Figure 3*; a score higher than 0 was considered to be visualized and to satisfy the criteria for diagnostic quality.

In addition, the lengths of the RCA, left anterior

Table 2 Basal characteristics of children with known or suspected CAAs

Variable	Children with known or suspected CAAs (n=65)
Age (years)	8.5±4.4
Heart rate (beats/min)	92±18
BMI (kg/m^2)	17.4±3.5
Male	37 (56.9)
Female	28 (43.1)
Sedation	21 (32.3)
Awake	44 (67.7)
The classification of CAAs based on CCTA or ICA	
High tubular aorta	7
Acute angle	3
LCX to sinus	5
LCA to the right sinus	3
RCA to the left sinus	3
Myocardial bridge	10
CA to the aorta wall	2
ALCAPA	1

Normally distributed data are given as mean ± SD or n (%). CAA, coronary artery anomaly; BMI, body mass index; CCTA, coronary computed tomography angiography; ICA, invasive coronary angiography; LCX, left circumflex coronary artery; LCA, left coronary artery; RCA, right coronary artery; CA, coronary artery; ALCAPA, left coronary artery arising from the pulmonary artery; SD, standard deviation.

descending coronary artery (LAD), and left circumflex coronary artery (LCX) were measured on the CPR images. Finally, the vessel sharpness representing the signal change at the vessel border was measured on the proximal LCX, RCA, and left main coronary artery (LM)-LAD. In accordance with a previous study, a higher calculated value represented better vessel visualization (29).

Diagnostic performance analysis

The results of CCTA and ICA were evaluated by a radiologist (Wen L), who had 8 years of experience in cardiac imaging and was blinded to the clinical information and the result of CMRA. After the diagnostic work was completed, the sensitivity, specificity, positive predictive value (PPV), and negative predictive value (NPV) of sNAV-CMRA and dNAV-CMRA were calculated using CCTA or ICA as references for CAAs and ACAOS.

Statistical analysis

The data were analyzed using SPSS (version 25.0, IBM Corp., Armonk, NY, USA). Normally distributed quantitative data are depicted as the mean ± standard deviation, and nonnormally distributed data are expressed as the median with interquartile range. The success rate, scan time, and image quality were compared between the two sequences using paired *t*-test or Wilcoxon signed rank test. The McNemar chi-squared test was performed to compare the specificity and sensitivity of sNAV-CMRA and dNAV-CMRA. A four-fold-table chi-squared test was used to compare the two sequences' PPV and NPV. A 2-tailed P value <0.05 was considered statistically significant.

Results

Initially, 69 patients were eligible for inclusion in this study, but 4 were excluded for poor cooperation (n=1) and arrhythmia (n=3), leaving 65 patients for examination under both sequences. Of these pediatric patients, 4 (12.2±2.6 years) failed to complete the dNAV-CMRA examination, and 3 underwent sNAV-CMRA after dNAV-CMRA; for these 3 patients, the dNAV-CMRA examination was interrupted by operators because of diaphragmatic drift over time due to low acquisition efficiency; and for 1 of these patients, in whom sNAV-CMRA was performed before dNAV-CMRA, the examination was interrupted due to patient noncompliance and movement during the test. These 4 pediatric patients were excluded from the analysis, and all of them underwent CMRA when awake, with the average acquisition efficiency being 21.5%±3.4%. Thus, the final study group consisted of 61 patients (age 8.3±4.4 years), of whom 40 (11.0±1.8 years) underwent CMRA when awake and 21 (3.4±2.3 years) underwent CMRA when sedated. All patients were in the sinus rhythm, and the average heart rate during scan acquisition was 92±18 beats/min. Moreover, 39 (10.2±3.6 years) of the patients underwent CCTA or ICA, the findings of which were used to evaluate the diagnostic performance. Within 2 weeks, 87.2% (34/39) of the patients underwent CCTA while 12.8% (5/39) underwent ICA. The patients' characteristics and the distribution of classified CAAs are detailed in *Table 2*. The success rate of sNAV-CMRA (65/65, 100%) was higher than that of dNAV-CMRA (61/65, 93.8%) (P<0.001). The scan time of sNAV-

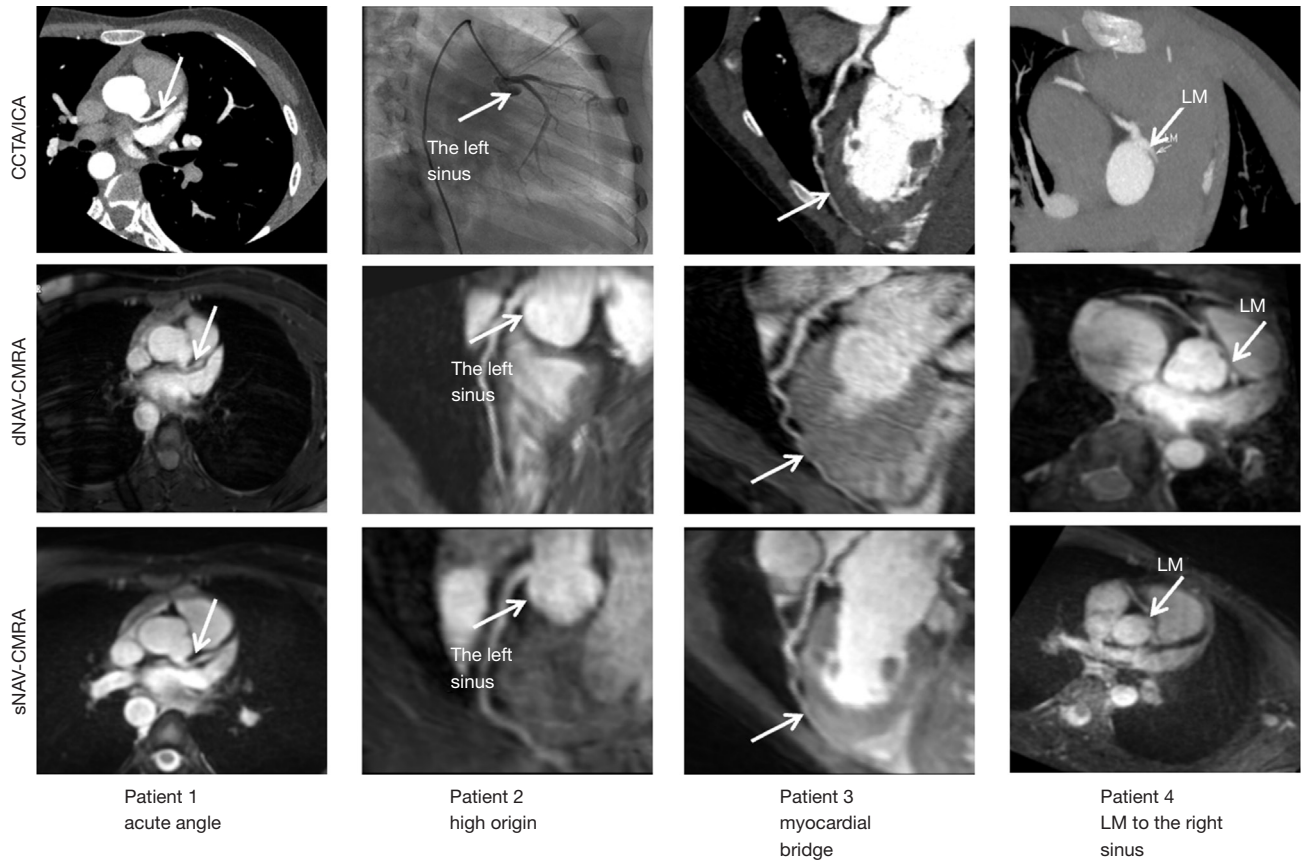

Figure 4 Representative images of CAAs in CCTA/ICA, dNAV-CMRA and sNAV-CMRA. Patient 1: a 17-year-old patient was diagnosed with acute angle. Patient 2: a 14-year-old patient was diagnosed with a high origin of the coronary artery. Patient 3: an 8-year-old patient was diagnosed with myocardial bridge coronary. Patient 4: a 13-year-old patient was diagnosed with the left coronary artery originating from the right coronary artery sinus, which was slightly compressed by the ascending aorta and pulmonary artery. The arrows indicate the lesion's location. CCTA, coronary computed tomography angiography; ICA, invasive coronary angiography; dNAV-CMRA, diaphragmatic-navigated coronary magnetic resonance angiography; sNAV-CMRA, self-navigated coronary magnetic resonance angiography; LM, left main coronary artery; CAA, coronary artery anomaly.

CMRA (7.3±2.5 min) was significantly shorter than that of dNAV-CMRA (9.1±3.6 min) (P=0.002).

Image quality

Figure 4 shows the representative images of CAAs in CCTA/ICA, dNAV-CMRA and sNAV-CMRA. Quantitative and qualitative analysis of image quality between two sequences are summarized in *Table 3* and shown in *Figure 5*. In the study cohort, coronary artery origins were depicted in 98.4% (60/61) of patients, and there was no difference in the vessel visualized ratio between these two sequences (all P values >0.05). The visible scores of the LM, LCX, proximal and middle RCA, and LAD segments showed no statistically significant difference between the two sequences (all P values >0.05). However, dNAV-CMRA obtained higher scores for the distal RCA and LAD (P<0.050).

The LAD, LCX, and RCA lengths (*Table 3*) showed no differences between the two sequences (P>0.050), and the sharpness (*Table 3*) of the LCX showed no significant difference between dNAV-CMRA (3.6±1.6) and sNAV-CMRA (3.4±2.2) (P=0.176). In contrast, the sharpness of the RCA and LAD was significantly improved (both P values <0.050) under dNAV-CMRA (3.6±1.6 and 4.0±2.0, respectively) compared with sNAV-CMRA (3.2±1.5 and 3.3±2.2, respectively).

Table 3 Quantitative and qualitative analysis of image quality between two sequences

Parameter	dNAV-CMRA (n=61)	sNAV-CMRA (n=61)	P
Visualization of coronary arteries			
LM	3.4±0.9	3.3±1.1	0.152
LAD proximal	3.2±1.1	3.2±1.2	0.419
LAD mid	3.0±1.3	2.8±1.3	0.376
LAD distal	2.3±1.2	1.9±1.3	0.015*
RCA proximal	3.3±1.1	3.2±1.1	0.142
RCA mid	3.2±1.3	3.0±1.3	0.095
RCA distal	2.6±1.5	2.0±1.4	0.004*
LCX proximal	3.1±1.2	3.0±1.2	0.611
LCX distal	2.3±1.4	2.3±1.4	0.492
Vessel length (mm)			
RCA	77.1±25.2	73.5±24.4	0.080
LAD	79.2±23.8	77.5±29.1	0.274
LCX	67.7±21.4	67.0±21.0	0.800
Vessel sharpness			
RCA	3.6±1.6	3.2±1.5	0.032*
LM-LAD	4.0±2.0	3.3±2.2	0.003*
LCX	3.6±1.6	3.4±2.2	0.176

Data are presented as mean ± SD. *, P<0.05. dNAV-CMRA, diaphragmatic-navigated coronary magnetic resonance angiography; sNAV-CMRA, self-navigated coronary magnetic resonance angiography; LM, left main coronary artery; LAD, left anterior descending coronary artery; RCA, right coronary artery; LCX, left circumflex coronary artery; SD, standard deviation.

The diagnostic performance of sNAV-CMRA and dNAV-CMRA

Diagnostic-quality images were obtained in all 39 patients who underwent CCTA or ICA. Among these pediatric patients, 79.48% (31/39) were diagnosed with CAAs using CCTA or ICA. Both CMRA sequences correctly recognized 96.8% (30/31) of CAAs diagnosed with CCTA or ICA. The sensitivity, specificity, PPV, and NPV of the detection CAAs were no different between sNAV-CMRA (96.8%, 100%, 100%, and 88.9%, respectively) and sNAV-CMRA (96.8%, 100%, 100%, and 88.9%, respectively) (all P values >0.99). The sensitivity, specificity, PPV, and NPV of the detection ACAOS also showed no difference between sNAV-CMRA (100%, 100%, 100%, and 100%, respectively) and dNAV-CMRA (100%, 100%, 100%, and 100%, respectively) (all P values >0.99).

Discussion

This is the first study to investigate the clinical application value of 3T CMRA in pediatric patients with CAAs. The key findings are as follows: (I) sNAV-CMRA provided a shorter scan time and higher success rate than did dNAV-CMRA. (II) There was no significant difference in vessel length of all coronary arteries, the visual score, or the vessel sharpness of LCX. The visual score and vessel sharpness of the RCA and LAD using dNAV-CMRA were superior to that using sNAV-CMRA. (III) We found that both sequences had similar diagnostic accuracy in detecting CAAs.

Compared to using dNAV, using sNAV had a significantly reduced scan time. The sNAV approach achieved 100% respiratory scan efficiency without relying on operator expertise, and the scan time was highly predictable because it depended on the average heart rate of the patient

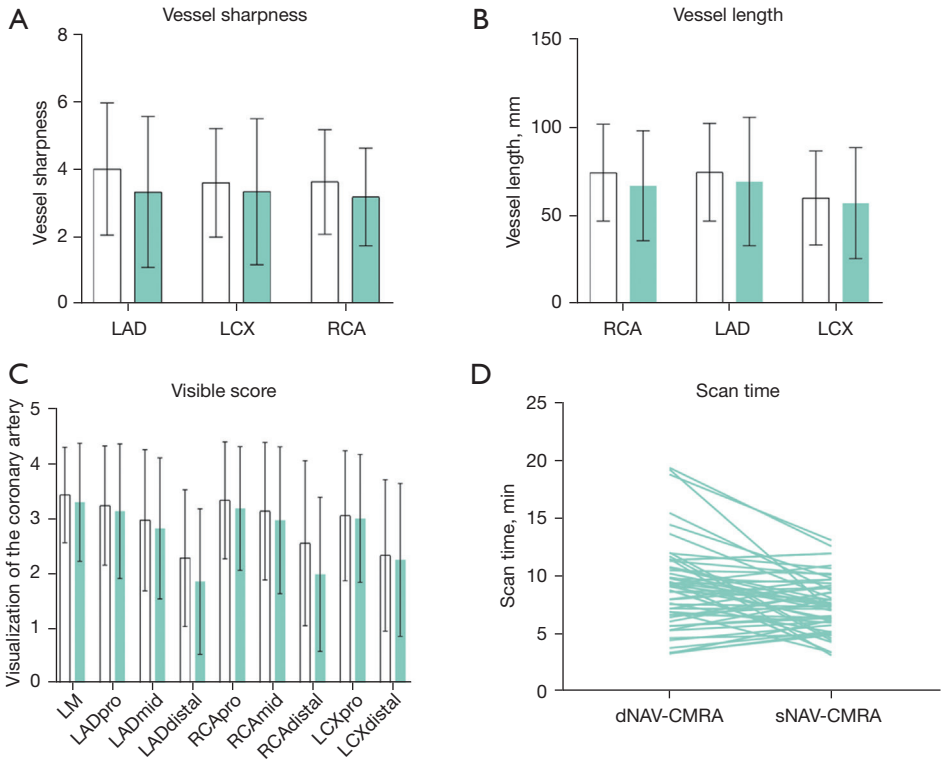

Figure 5 Qualitative and quantitative analysis of coronary arteries between sNAV-CMRA and dNAV-CMRA in pediatric patients with suspected CAAs. (A) Vessel sharpness; (B) vessel length; (C) visualization of the coronary artery; (D) scan time. LAD, left anterior descending coronary artery; LCX, left circumflex coronary artery; RCA, right coronary artery; LM, the left main coronary artery; dNAV-CMRA, diaphragmatic-navigated coronary magnetic resonance angiography; sNAV-CMRA, self-navigated coronary magnetic resonance angiography; CAA, coronary artery anomaly.

(17,21). The conventional dNAV approach, however, is associated with unpredictable and prolonged scan time due to dNAV-CMRA gate image acquisition discarding and reacquiring data falling outside a prerespiratory window. Furthermore, inefficient data acquisition due to irregular breathing patterns and poor navigator positioning can also lead to prolonged scan time (11,30). The second major factor that impacts the scan time is the k-space sampling technique. The dNAV is accelerated by a factor of 2 with GRAPPA, while sNAV is accelerated by a factor of 5 with undersampling, and the amount of data to be filled in the k-space in sNAV is much more than that in dNAV. It should be emphasized that the scan time of sNAV could be longer than that of dNAV if the acceleration factor and similar acquisition efficiency had been matched between these two sequences. Our study also found a reduction in the scan time of dNAV-CMRA compared with previous studies in adults, which approximately ranged from 10 minutes to 1 hour (9,31); this may be attributable to the rapid and superficial respiration pattern of children in contrast to the slower and deeper pattern observed in adults. Additionally, 21 pediatric patients underwent the examination under sedation, resulting in a more stable breathing pattern, which might have significantly improved the acquisition efficiency and shortened the scan time.

Regarding examination success rate, sNAV-CMRA exhibited a significantly higher success rate than did dNAV-CMRA. sNAV-CMRA directly estimates respiratory motion in the heart, resulting in a 100% scan success rate, and the shorter scan time of sNAV is also a factor that contributes to a higher success rate (21). The success rate of dNAV-CMRA ranged from 85–92% in previous studies (32-34), which is comparable with that of our investigation. Several factors can cause the failure of dNAV-CMRA examination. First, the prolonged acquisition time can increase susceptibility to movement, leading to irregular respiratory patterns and diaphragmatic drift, often resulting in scan failure (31,35). Additionally, complex examination planning,

such as inadequate positioning of the navigator or inability to recognize relatively still periods in the cardiac cycle, leads to scanning failure (36). Our study suggests that the higher scan success rate and shorter scan time of sNAV-CMRA can benefit pediatric patients who may exhibit poorer cooperation and tolerance toward more extended examinations than it can adults.

Although the visual score and vessel sharpness of the RCA and LAD using dNAV-CMRA was superior to that of sNAV-CMRA, there was no significant difference in vessel length in any of coronary arteries, the visual score, or the vessel sharpness of LCX, suggesting that both can be used to identify the spatial position of the anomalous origin and course of the main coronary branches. The potential influences of image quality are as follows. First, motion correction strategies affect image quality. Both sequences of correct respiratory motion in the superior–inferior direction have been proven insufficient because they do not consider remaining orientations or non-rigid deformations (30). However, dNAV-CMRA uses data that fall in a small acquisition window to reduce respiratory artifacts, while sNAV-CMRA uses the entire respiratory range for motion correction; this might have resulted in the inclusion of some outlier respiratory positions in the reconstruction and decreased the image quality of sNAV-CMRA (12). Another factor that might have affected image quality is the k-space sampling strategy. The 3D radial trajectories used by sNAV-CMRA had a higher sampling density near the center of the k-space than near the periphery, which might have impacted the clarity of the vessel boundary (20). Furthermore, the data sNAV-CMRA used to correct respiratory artefacts were directly extracted from the ventricular blood pool, and the poor image quality might have been due to the low tracking efficiency of the self-navigation technique in pediatric patients who were young children with smaller cardiac structures (37).

The clinical significance of CAAs varies substantially depending on the affected artery and its origin and course. Therefore, precise evaluation of the origin and proximal course of the coronary arteries is essential for determining the clinical significance of any potential CAAs (38). The diagnostic performance of CMRA for CAAs has shown considerable variation across different studies, which may be attributed to the presence or absence of contrast agents, and the heterogeneity in the acquisition sequences used. Albrecht *et al.* conducted a study with 21 pediatric patients using free-breathing, sNAV-CMRA at 1.5T as the imaging modality and CT angiography as the reference standard and reported a sensitivity and specificity of 71% and 92% for the detection of ACAOS, respectively, and 92% and for 92% the detection of CAAs, respectively (18). In their study of a cohort with 100 pediatric patients, Tangcharoen *et al.* found that CAAs could be confirmed or excluded in all cases using 1.5T contrast-enhanced dNAV-CMRA (9). Piccini *et al.* reported that 1.5T contrast-enhanced sNAV-CMRA could confirm or exclude CAAs in all cases in a cohort of 78 adults, including 17 patients with CAAs (17). In our study, the diagnostic performance of both dNAV- and sNAV-CMRA sequences for CAAs was comparable to those of the previous studies. Both sequences successfully confirmed or excluded ACAOS, which is considered a high-risk factor for ischemia and sudden death. Our study demonstrated that 3T sNAV-CMRA and dNAV-CMRA achieved high sensitivity and specificity in pediatric patients with CAAs. Although the image quality of dNAV-CMRA was slightly higher than that of sNAV-CMRA, the diagnostic accuracy was similar to that of sNAV-CMRA. Moreover, there were certain challenges in the scanning procedure of dNAV-CMRA, while sNAV-CMRA could simplify the scanning process to shorten the scan time of CMRA of the CAAs in pediatric patients.

There were some limitations in our study. First, the patient cohort was relatively small and from a single center, which possibly introduced selection bias. Second, only 63.93% (39/61) of the pediatric patients could be used to calculate diagnostic accuracy due to CCTA and ICA exposure to high radiation doses, iodinated contrast agents, or invasiveness. Third, the SNR did not differ between the two sequences in the phantom experiment. However, currently, we only have a water phantom and cannot calculate the sharpness with this water phantom, as it only has a single type of contrast. Although part of the image parameters in the two sequences were not wholly matched, we compared dNAV and sNAV in whole-heart CMRA using optimized protocols that balanced the spatial resolution, SNR, and scan time in clinical practice. Finally, both sequences investigated in this study corrected the motion in the simplistic superior-inferior direction, which is insufficient to account for respiratory-induced complex displacement of the heart. To reduce the remaining source of error in the superior-inferior motion correction, Abdi *et al.* introduced deep learning, which is an effective method to compensate for respiratory motion-induced signal loss and phase corruption (39). Prior work developing sNAV cine displacement encoding with stimulated echoes introduced the match-making method, which effectively

addresses the suppression of the T1 echo and corrects for in-plane position shifts due to breathing (40). Furthermore, advanced CMRA motion compensation strategies, such as image-based self-navigation (iNAV)-CMRA, have been proposed to improve image quality and reduce the scan time. Compared with sNAV, iNAV-CMRA provided similar efficiency, predictable scan times, and ease of use while also enabling 3D affine or 3D non-rigid reconstruction. It was reported that iNAV significantly improved the image quality (41), but validation in 3T CMRA and with larger cohorts has not yet been completed.

Conclusions

Our findings demonstrated that both sNAV-CMRA and dNAV-CMRA provide clinical application value in pediatric patients with CAAs and have similar diagnostic performance. Compared to dNAV-CMRA, sNAV-CMRA allows for a simpler scanning procedure although the image quality of the sNAV-CMRA is slightly inferior.

Acknowledgments

Funding: This work was supported by the National Natural Science Foundation of China (Nos. 82120108015, 82102020, 82071874, and 81971586); the Sichuan Science and Technology Program (Nos. 2022YFS0178, 2020YJ0029, and 2017TD0005); the Clinical Research Grant of Chinese Society of Cardiovascular Disease (CSC) of 2019 (No. HFCSC2019B01); and the Scientific Research Project of Sichuan Health Planning Committee (No. 21PJ048).

Footnote

Conflicts of Interest: All authors have completed the ICMJE uniform disclosure form (available at https://qims.amegroups.com/article/view/10.21037/qims-23-556/coif). DP was an employee of Siemens Healthcare AG, Lausanne, Switzerland, throughout his involvement in the study. XZ was an employee of Siemens Healthineers Ltd., Shanghai, China, throughout her involvement in the study. JA was an employee of Siemens Shenzhen Magnetic Resonance Ltd., Shenzhen, China, throughout her involvement in the study. The other authors have no conflicts of interest to declare.

Ethical Statement: The authors are accountable for all aspects of the work in ensuring that questions related to the accuracy or integrity of any part of the work are appropriately investigated and resolved. This prospective study was conducted in accordance with the Declaration of Helsinki (as revised in 2013) and approved by the Ethics Committee of Sichuan University (No. KL108). Written informed consent was obtained from each patient's legal guardian before enrollment.

References

1. Pérez-Pomares JM, de la Pompa JL, Franco D, Henderson D, Ho SY, Houyel L, Kelly RG, Sedmera D, Sheppard M, Sperling S, Thiene G, van den Hoff M, Basso C. Congenital coronary artery anomalies: a bridge from embryology to anatomy and pathophysiology--a position statement of the development, anatomy, and pathology ESC Working Group. Cardiovasc Res 2016;109:204-16.
2. Schiavone M, Gobbi C, Gasperetti A, Zuffi A, Forleo GB. Congenital Coronary Artery Anomalies and Sudden Cardiac Death. Pediatr Cardiol 2021;42:1676-87.
3. Ripley DP, Saha A, Teis A, Uddin A, Bijsterveld P, Kidambi A, McDiarmid AK, Sivananthan M, Plein S, Pennell DJ, Greenwood JP. The distribution and prognosis of anomalous coronary arteries identified by cardiovascular magnetic resonance: 15 year experience from two tertiary centres. J Cardiovasc Magn Reson 2014;16:34.
4. Ghadri JR, Kazakauskaite E, Braunschweig S, Burger IA, Frank M, Fiechter M, Gebhard C, Fuchs TA, Templin C, Gaemperli O, Lüscher TF, Schmied C, Kaufmann PA. Congenital coronary anomalies detected by coronary computed tomography compared to invasive coronary angiography. BMC Cardiovasc Disord 2014;14:81.
5. Gentile F, Castiglione V, De Caterina R. Coronary Artery Anomalies. Circulation 2021;144:983-96.
6. Leiner T, Bogaert J, Friedrich MG, Mohiaddin R, Muthurangu V, Myerson S, Powell AJ, Raman SV, Pennell DJ. SCMR Position Paper (2020) on clinical indications for cardiovascular magnetic resonance. J Cardiovasc Magn Reson 2020;22:76.

7. Valsangiacomo Buechel ER, Grosse-Wortmann L, Fratz S, Eichhorn J, Sarikouch S, Greil GF, et al. Indications for cardiovascular magnetic resonance in children with congenital and acquired heart disease: an expert consensus paper of the Imaging Working Group of the AEPC and the Cardiovascular Magnetic Resonance Section of the EACVI. Eur Heart J Cardiovasc Imaging 2015;16:281-97.
8. Fogel MA, Anwar S, Broberg C, Browne L, Chung T, Johnson T, Muthurangu V, Taylor M, Valsangiacomo-Buechel E, Wilhelm C. Society for Cardiovascular Magnetic Resonance/European Society of Cardiovascular Imaging/American Society of Echocardiography/ Society for Pediatric Radiology/North American Society for Cardiovascular Imaging Guidelines for the use of cardiovascular magnetic resonance in pediatric congenital and acquired heart disease: Endorsed by The American Heart Association. J Cardiovasc Magn Reson 2022;24:37.
9. Tangcharoen T, Bell A, Hegde S, Hussain T, Beerbaum P, Schaeffter T, Razavi R, Botnar RM, Greil GF. Detection of coronary artery anomalies in infants and young children with congenital heart disease by using MR imaging. Radiology 2011;259:240-7.
10. Albrecht MH, Varga-Szemes A, Schoepf UJ, Apfaltrer G, Xu J, Jin KN, Hlavacek AM, Chowdhury SM, Suranyi P, Tesche C, De Cecco CN, Piccini D, Stuber M, Ginami G, Vogl TJ, Nutting A. Coronary artery assessment using self-navigated free-breathing radial whole-heart magnetic resonance angiography in patients with congenital heart disease. Eur Radiol 2018;28:1267-75.
11. Bustin A, Rashid I, Cruz G, Hajhosseiny R, Correia T, Neji R, Rajani R, Ismail TF, Botnar RM, Prieto C. 3D whole-heart isotropic sub-millimeter resolution coronary magnetic resonance angiography with non-rigid motion-compensated PROST. J Cardiovasc Magn Reson 2020;22:24.
12. Piccini D, Littmann A, Nielles-Vallespin S, Zenge MO. Spiral phyllotaxis: the natural way to construct a 3D radial trajectory in MRI. Magn Reson Med 2011;66:1049-56.
13. Stehning C, Börnert P, Nehrke K, Eggers H, Stuber M. Free-breathing whole-heart coronary MRA with 3D radial SSFP and self-navigated image reconstruction. Magn Reson Med 2005;54:476-80.
14. Bastiaansen JAM, van Heeswijk RB, Stuber M, Piccini D. Noncontrast free-breathing respiratory self-navigated coronary artery cardiovascular magnetic resonance angiography at 3 T using lipid insensitive binomial off-resonant excitation (LIBRE). J Cardiovasc Magn Reson 2019;21:38.
15. Lu H, Guo J, Zhao S, Yang S, Ma J, Ge M, Chen Y, Zeng M, Jin H. Assessment of Non-contrast-enhanced Dixon Water-fat Separation Compressed Sensing Whole-heart Coronary MR Angiography at 3.0 T: A Single-center Experience. Acad Radiol 2022;29 Suppl 4:S82-90.
16. Soleimanifard S, Stuber M, Hays AG, Weiss RG, Schär M. Robust volume-targeted balanced steady-state free-precession coronary magnetic resonance angiography in a breathhold at 3.0 Tesla: a reproducibility study. J Cardiovasc Magn Reson 2014;16:27.
17. Piccini D, Monney P, Sierro C, Coppo S, Bonanno G, van Heeswijk RB, Chaptinel J, Vincenti G, de Blois J, Koestner SC, Rutz T, Littmann A, Zenge MO, Schwitter J, Stuber M. Respiratory self-navigated postcontrast whole-heart coronary MR angiography: initial experience in patients. Radiology 2014;270:378-86.
18. Albrecht MH, Varga-Szemes A, Schoepf UJ, Nance JW, De Cecco CN, De Santis D, Tesche C, Eid MH, Penmetsa M, Lesslie VW, Piccini D, Goeller M, Wichmann JL, Vogl TJ, Chowdhury SM, Nutting A, Hlavacek AM. Diagnostic Accuracy of Noncontrast Self-navigated Free-breathing MR Angiography versus CT Angiography: A Prospective Study in Pediatric Patients with Suspected Anomalous Coronary Arteries. Acad Radiol 2019;26:1309-17.
19. Zhou ZQ, Wen LY, Fu C, Yang Z, Fu H, Xu R, Zhang L, Xu K, Zhou B, Shi XQ, Guo YK. Association of left ventricular systolic dysfunction with coronary artery dilation in Kawasaki disease patients: Assessment with cardiovascular magnetic resonance. Eur J Radiol 2021;145:110039.
20. Heerfordt J, Stuber M, Maillot A, Bianchi V, Piccini D. A quantitative comparison between a navigated Cartesian and a self-navigated radial protocol from clinical studies for free-breathing 3D whole-heart bSSFP coronary MRA. Magn Reson Med 2020;84:157-69.
21. Piccini D, Littmann A, Nielles-Vallespin S, Zenge MO. Respiratory self-navigation for whole-heart bright-blood coronary MRI: methods for robust isolation and automatic segmentation of the blood pool. Magn Reson Med 2012;68:571-9.
22. Lauenstein TC, Sharma P, Hughes T, Heberlein K, Tudorascu D, Martin DR. Evaluation of optimized inversion-recovery fat-suppression techniques for T2-weighted abdominal MR imaging. J Magn Reson Imaging 2008;27:1448-54.
23. Griswold MA, Jakob PM, Heidemann RM, Nittka M, Jellus V, Wang J, Kiefer B, Haase A. Generalized autocalibrating partially parallel acquisitions (GRAPPA). Magn Reson Med 2002;47:1202-10.
24. Wang Y, Riederer SJ, Ehman RL. Respiratory motion

of the heart: kinematics and the implications for the spatial resolution in coronary imaging. Magn Reson Med 1995;33:713-9.
25. Rosen BR, Wedeen VJ, Brady TJ. Selective saturation NMR imaging. J Comput Assist Tomogr 1984;8:813-8.
26. Brittain JH, Hu BS, Wright GA, Meyer CH, Macovski A, Nishimura DG. Coronary angiography with magnetization-prepared T2 contrast. Magn Reson Med 1995;33:689-96.
27. Ginami G, Bonanno G, Schwitter J, Stuber M, Piccini D. An iterative approach to respiratory self-navigated whole-heart coronary MRA significantly improves image quality in a preliminary patient study. Magn Reson Med 2016;75:1594-604.
28. Abbara S, Blanke P, Maroules CD, Cheezum M, Choi AD, Han BK, Marwan M, Naoum C, Norgaard BL, Rubinshtein R, Schoenhagen P, Villines T, Leipsic J. SCCT guidelines for the performance and acquisition of coronary computed tomographic angiography: A report of the society of Cardiovascular Computed Tomography Guidelines Committee: Endorsed by the North American Society for Cardiovascular Imaging (NASCI). J Cardiovasc Comput Tomogr 2016;10:435-49.
29. Vu CT, Phan TD, Chandler DM. S3: a spectral and spatial measure of local perceived sharpness in natural images. IEEE Trans Image Process 2012;21:934-45.
30. Roy CW, Heerfordt J, Piccini D, Rossi G, Pavon AG, Schwitter J, Stuber M. Motion compensated whole-heart coronary cardiovascular magnetic resonance angiography using focused navigation (fNAV). J Cardiovasc Magn Reson 2021;23:33.
31. Fotaki A, Munoz C, Emanuel Y, Hua A, Bosio F, Kunze KP, Neji R, Masci PG, Botnar RM, Prieto C. Efficient non-contrast enhanced 3D Cartesian cardiovascular magnetic resonance angiography of the thoracic aorta in 3 min. J Cardiovasc Magn Reson 2022;24:5.
32. Sakuma H, Ichikawa Y, Suzawa N, Hirano T, Makino K, Koyama N, Van Cauteren M, Takeda K. Assessment of coronary arteries with total study time of less than 30 minutes by using whole-heart coronary MR angiography. Radiology 2005;237:316-21.
33. Sakuma H, Ichikawa Y, Chino S, Hirano T, Makino K, Takeda K. Detection of coronary artery stenosis with whole-heart coronary magnetic resonance angiography. J Am Coll Cardiol 2006;48:1946-50.
34. Kato S, Kitagawa K, Ishida N, Ishida M, Nagata M, Ichikawa Y, Katahira K, Matsumoto Y, Seo K, Ochiai R, Kobayashi Y, Sakuma H. Assessment of coronary artery disease using magnetic resonance coronary angiography: a national multicenter trial. J Am Coll Cardiol 2010;56:983-91.
35. Ishida M, Schuster A, Takase S, Morton G, Chiribiri A, Bigalke B, Schaeffter T, Sakuma H, Nagel E. Impact of an abdominal belt on breathing patterns and scan efficiency in whole-heart coronary magnetic resonance angiography: comparison between the UK and Japan. J Cardiovasc Magn Reson 2011;13:71.
36. Correa Londono M, Trussardi N, Obmann VC, Piccini D, Ith M, von Tengg-Kobligk H, Jung B. Radial self-navigated native magnetic resonance angiography in comparison to navigator-gated contrast-enhanced MRA of the entire thoracic aorta in an aortic patient collective. J Cardiovasc Magn Reson 2021;23:94.
37. Monney P, Piccini D, Rutz T, Vincenti G, Coppo S, Koestner SC, Sekarski N, Di Bernardo S, Bouchardy J, Stuber M, Schwitter J. Single centre experience of the application of self navigated 3D whole heart cardiovascular magnetic resonance for the assessment of cardiac anatomy in congenital heart disease. J Cardiovasc Magn Reson 2015;17:55.
38. Cheezum MK, Liberthson RR, Shah NR, Villines TC, O'Gara PT, Landzberg MJ, Blankstein R. Anomalous Aortic Origin of a Coronary Artery From the Inappropriate Sinus of Valsalva. J Am Coll Cardiol 2017;69:1592-608.
39. Abdi M, Bilchick KC, Epstein FH. Compensation for respiratory motion-induced signal loss and phase corruption in free-breathing self-navigated cine DENSE using deep learning. Magn Reson Med 2023;89:1975-89.
40. Cai X, Epstein FH. Free-breathing cine DENSE MRI using phase cycling with matchmaking and stimulated-echo image-based navigators. Magn Reson Med 2018;80:1907-21.
41. Velasco Forte MN, Valverde I, Prabhu N, Correia T, Narayan SA, Bell A, Mathur S, Razavi R, Hussain T, Pushparajah K, Henningsson M. Visualization of coronary arteries in paediatric patients using whole-heart coronary magnetic resonance angiography: comparison of image-navigation and the standard approach for respiratory motion compensation. J Cardiovasc Magn Reson 2019;21:13.

Cite this article as: Azhe S, Li X, Zhou Z, Fu C, Wang Y, Zhou X, An J, Piccini D, Bastiaansen J, Guo Y, Wen L. Comparison between diaphragmatic-navigated and self-navigated coronary magnetic resonance angiography at 3T in pediatric patients with congenital coronary artery anomalies. Quant Imaging Med Surg 2023. doi: 10.21037/qims-23-556

Supplementary

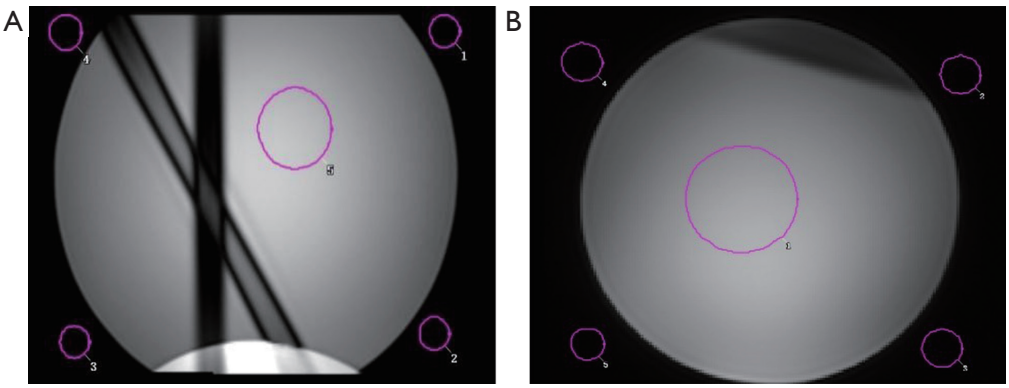

Figure S1 The signal-to-noise ratio was not different between the dNAV-CMRA and the sNAV-CMRA (dNAV-CMRA: 310; sNAV-CMRA: 313) in the phantom. The purple circles indicate region of interest. dNAV-CMRA, diaphragmatic-navigated coronary magnetic resonance angiography; sNAV-CMRA, self-navigated coronary magnetic resonance angiography.

https://dx.doi.org/10.21037/qims-23-556